

Dalton Transactions

Accepted Manuscript



This is an *Accepted Manuscript*, which has been through the Royal Society of Chemistry peer review process and has been accepted for publication.

Accepted Manuscripts are published online shortly after acceptance, before technical editing, formatting and proof reading. Using this free service, authors can make their results available to the community, in citable form, before we publish the edited article. We will replace this *Accepted Manuscript* with the edited and formatted *Advance Article* as soon as it is available.

You can find more information about *Accepted Manuscripts* in the [Information for Authors](#).

Please note that technical editing may introduce minor changes to the text and/or graphics, which may alter content. The journal's standard [Terms & Conditions](#) and the [Ethical guidelines](#) still apply. In no event shall the Royal Society of Chemistry be held responsible for any errors or omissions in this *Accepted Manuscript* or any consequences arising from the use of any information it contains.

ARTICLE

Synthesis and Characterization of a Modified “Picket Fence” Porphyrin Complex — Stronger π Bonding Interactions between Fe(II) and Axial Ligands

Cite this: DOI: 10.1039/x0xx00000x

Received 00th January 2012,

Accepted 00th January 2012

DOI: 10.1039/x0xx00000x

www.rsc.org/Baiyin He,^a Charles E. Schulz^b and Jianfeng Li^{*a}

A new, modified “picket fence” porphyrin is synthesized and its bis(imidazole)-ligated iron(II) derivative [Fe(MbenTpivPP)(1-MeIm)₂] is investigated. X-ray structure determinations demonstrate that [Fe(MbenTpivPP)(1-MeIm)₂] has structural features of a near planar porphyrin plane, a relative perpendicular ligand orientation, and one unusually large absolute ligand orientation (φ). The combination of these features leads to a new type of species that is different from previously reported analogues. Further structural examination reveals a strong correlation between the mutual ligand orientations (θ) and the axial Fe—N_{Im} bond distances, which is detailed for the first time. Mössbauer spectroscopic characterization shows that the low spin derivative has a quadrupole splitting of 0.99 mm/s at 100K.

Introduction

Porphyrin models have been investigated to correlate the structure of heme centers with their physical and spectroscopic properties.¹ This strategy has been successful in the examination of the relative and absolute orientation of planar axial ligands of iron porphyrin complexes.² A good example that demonstrating the importance of axial ligand orientation is [Fe(III)(OEP)(3-CIPy)₂]ClO₄³ where two distinct crystalline polymorphs have been isolated.^{4,5} In these structures, the two pyridine planes maintained a relative parallel orientation, but the absolute orientation of the planes changed. In the first polymorph, the axial pyridine planes approximately bisect the N_p—Fe—N_p angles and an $S = 1/2 \rightleftharpoons S = 5/2$ equilibrium has been found.⁵ In the second polymorph, the two planar axial ligands nearly eclipses the Fe—N_p bond, and an intermediate spin state of iron was found.⁶

Substantial investigations had been done on the electronic structure of low spin iron(III) porphyrin complexes and the effect of the axial ligand orientation is relatively clear.⁷ Steric axial ligands such as 2-methylimidazole (or tetrakis(2,6-disubstituted phenyl)porphyrinates with bulky imidazoles⁸ or pyridines^{9,10}) are required to force the near perpendicular

orientation of planar axial ligands in Fe(III) porphyrinates. These iron(III) species display electron paramagnetic resonance (EPR) spectra with a characteristic signal at $g \geq 3.2$, that has been called “large g_{\max} ”¹¹ (or highly anisotropic low-spin, HALS¹²). The “large g_{\max} ” signal occurs for ferriheme complexes with $(d_{xy})^2(d_{xz}, d_{yz})^3$ electronic ground states when the axial ligands are in (near) perpendicular orientations;¹³ in contrast, low-spin species with axial ligands having relative parallel orientations exhibit rhombic EPR spectra with three g -values consistent with an electronic configuration of $(d_{xy})^2(d_{xz}, d_{yz})^3$.^{14,15} “Large g_{\max} ” signals are observed for complexes in which the splitting between the d_{xz} and d_{yz} orbitals is small; whereas rhombic signals are seen when the splitting between these two orbitals is larger.

It had been assumed that for low spin d⁶ Fe(II) porphyrinates with closed subshell configurations, two planar axial ligands would prefer to align themselves in mutually perpendicular orientations to maximize the π -bonding interactions between the filled $d\pi$ orbitals of Fe(II) and the π^* orbitals of the planar ligands. However, subsequent studies¹⁶ showed that such iron(II) derivatives were not as readily obtained as in the case of iron(III) species. Both steric axial ligands and a porphyrin with bulky peripheral groups are required. The structure of

[Fe(TMP)(2-MeHIm)₂] showed that the two axial ligands have a nearly perpendicular ligand orientation and a very ruffled porphyrin core. Mössbauer characterization showed that the complex had a large ΔE_Q of ~ 1.7 mm/s.¹⁷ These structural and electronic features are markedly different from a series of [Fe(TPP)(Im)₂] derivatives with parallel ligand orientations, near planar porphyrin planes and ΔE_Q of ~ 1.0 mm/s.¹⁸ In a recent study, the features of near planar porphyrin cores, perpendicular ligand orientations and ΔE_Q of ~ 1.0 mm/s were found for one species. The investigation led to the conclusion that the common geometric factor for a large ΔE_Q is a ruffled core conformation rather than ligand orientation.¹⁹

“Picket fence” porphyrin is one of the most successful models for oxyheme proteins.²⁰ The bulky pickets provide an efficient pocket for the bonding of O₂. Efforts have been made to modify the traditional “picket fence” porphyrin with the aim of changing the pocket polarity²¹ and/or to provide H-bonding interactions.²² Although much research has been done, a single-crystal structure which will give a direct picture of the molecular coordination sphere has never been presented for such modified “picket fence” porphyrin models. Recently in a large study of vibrational dynamics of iron porphyrins,²³ we reported three bis(imidazole)-ligated picket fence porphyrin complexes of [FeTpivPP(R-Im)₂] (R-Im = 1-MeIm, 1-EtIm and 1-Vinylim)¹⁹ and their oxygen adducts.²⁴ In this work, we present the synthesis of a new modified “picket fence” porphyrin and its iron derivatives. We also isolated the bis(imidazole)-ligated iron(II) product and determined the molecular structure. The unique structural features make it a new type among the known [Fe(II)(Porph)(L)₂] (L = planar nitrogen donor ligands) complexes. It has also been characterized by the application of multitemperature Mössbauer measurements.

Experimental

General Information.

All reactions were carried out using standard Schlenk techniques under argon unless otherwise noted. Mössbauer measurement were performed on a constant acceleration spectrometer from 25 to 295 K with optional small field. A sample for Mössbauer spectroscopy was prepared by immobilization of the crystalline material in Apiezon M grease. ¹H, ¹³C-¹H NMR spectra were run on BRUKER AV600. UV-vis spectra were obtained on a Perkin-Elmer Lambda-25 spectrometer.

Tetrahydrofuran (THF), benzene, hexanes were distilled from sodium and benzophenone ketyl; dichloromethane was distilled from CaH₂; chlorobenzene was washed with concentrated sulfuric acid and then water until the aqueous layer was neutral, dried with anhydrous MgSO₄, and distilled twice over P₂O₅ under argon. Pivaloyl chloride, benzoyl chloride, 2,6-lutidine and 1-methylimidazole were distilled under argon before use. ⁵⁷Fe₂O₃, zinc and mercury were used as received. *Meso*-

tetrakis(*o*-aminophenyl)porphyrin, *meso*-tetrakis($\alpha,\alpha,\alpha,\alpha$ -aminophenyl) porphyrin (H₂TamPP, **1**)²⁵ and *meso*-mono(α -aminophenyl)tri(α,α,α -pivalamidophenyl)porphyrin (H₂MamTpivPP, **2**)²⁶ were prepared according to a local modification of the reported synthesis.

Synthesis of H₂MamTpivPP (2). H₂TamPP (0.50 g, 0.74 mmol) and 0.25 mL of 2,6-lutidine were dissolved in 100 mL of CH₂Cl₂. Pivaloyl chloride (0.286 g, 2.36 mmol) and 0.25 mL of 2,6-lutidine in 15 mL of CH₂Cl₂ was added dropwise to the H₂TamPP solution over 3 h. After additional 8 h stirring, 10% NH₃·H₂O (250 mL) was added and the reaction solution was stirred for another hour. The organic layer was separated and the aqueous layer was extracted with CHCl₃ three times. The combined organic portion was dried over anhydrous Na₂SO₄ and evaporated to dryness. The resulting solid was dissolved in small amount of eluent and purified by chromatography on a silica gel column (300-400 mesh, 25 cm; CHCl₃:Et₂O: hexane = 4:1:0.15). The second main band was collected, evaporated to dryness and followed by recrystallization (dichloromethane-hexane) to give a purple solid product of 410 mg (30%).

Synthesis of H₂MbenTpivPP (3). Freshly distilled benzoyl chloride (4 mL, 34.72 mmol) and 0.5 mL 2,6-lutidine was dissolved in 20 mL dichloromethane. The solution was slowly dropped into a dichloromethane solution (30 mL) of H₂MamTpivPP (500 mg, 0.54 mmol) and 0.3 mL of 2,6-lutidine. The mixture was stirred at ambient temperature overnight, concentrated by a rotary evaporator and filtered to give purple solid product. The crude product was chromatographed on a silica gel column (300-400 mesh, 20 cm; CHCl₃:Et₂O: hexane = 4:1:0.15). The main band was collected and recrystallized from dichloromethane-hexane to yield ~ 250 mg product (0.243 mmol, 45%). ¹H NMR (600MHz, CDCl₃, TMS): δ -2.59 (s, 2H, NH_{pyrr}), -0.04 (s, 18H, CH₃), 0.07 (s, 9H, CH₃), 6.33–6.39 (t, J = 7.7 Hz, 2H, CH_{ben}), 6.44–6.50 (d, J = 7.6 Hz, 2H, CH_{ben}), 6.75–6.81 (t, J = 7.3 Hz, 1H, CH_{ben}), 7.42–7.63 (m, 6H, CH_{aryl}), 7.76–8.05 (m, 10H, CH_{aryl}), 8.67–8.72 (t, J = 7.6 Hz, 3H, NH_{piv} and CH _{β pyrr}), 8.80–8.90 (d, J = 20.5 Hz, 9H, NH_{piv} and CH _{β pyrr}). ¹³C-¹H NMR (150MHz, CDCl₃, TMS): ¹H NMR: δ _H -0.03, 0.07 (CH₃), 6.36, 6.47, 6.78 (H_{ben}), 7.49, 7.54, 7.84, 7.85, 7.90, 7.95 (H_{aryl}), 8.70, 8.84, 8.86 (H _{β pyrr}); ¹³C NMR: δ _C 26.28, 26.40 (CH₃), 125.94, 125.96, 127.86 (C_{ben}), 123.13, 123.37, 130.14, 130.28, 134.42, 134.70, 134.71 (C_{aryl}), 121.06, 121.07, 131.69 (C_{pyrr}).

Synthesis of [Fe(MbenTpivPP)Cl] (4). Chlorobenzene solution of H₂MbenTpivPP (250 mg, 0.243 mmol) and 2,6-lutidine (0.4 mL) was transferred to anhydrous FeCl₂ (0.31 g, 2.43 mmol) by cannula. The reaction was stirred at 65°C for 10 h till the reaction was completed (monitored by TLC). The solvent was evaporated and the residue was dissolved in CHCl₃ and washed with several portions of diluted hydrochloric acid solution. The organic layer was dried over anhydrous Na₂SO₄ and evaporated. The resulting solid was purified on a silica gel column (300-400 mesh; CHCl₃:Et₂O: hexane = 4:1:0.15) and the main band was collected. After evaporation, the solid was recrystallized from CHCl₃-hexane to give 220 mg of

[Fe(MbenTpivPP)Cl] (0.196 mmol, 80.8%). UV-vis (CHCl₃): 417.6, 507.2, 577.0, 647.0, 674.0 nm.

Synthesis of [Fe(MbenTpivPP)(1-MeIm)₂] (6). [Fe(MbenTpivPP)Cl] (18 mg, 0.016 mmol) and zinc amalgam (10% zinc, 1 mL) were dried in vacuum for 2 h. Benzene (~8 mL) was transferred in and the mixture was stirred overnight to get [Fe(II)(MbenTpivPP)] (5). After 2 hours standing, the red solution was filtered to a new Schlenk and 1-MeIm (0.1 mL) was added to form complex (6). The reaction was stirred for 1 h under argon atmosphere, hexanes was then allowed to diffuse slowly into the solution. X-ray quality crystals were obtained several weeks later. UV-vis (benzene): 429.0, 535.6, 562.6 nm.

X-ray Structure Determinations.

The single crystal experiment was carried out on a BRUKER D8 VENTURE system with graphite monochromated Mo K α radiation ($\lambda = 0.71073 \text{ \AA}$). The crystalline samples were placed in inert oil, mounted on a glass pin, transferred to the cold gas stream of the diffractometer, and crystal data collected at 150 K. The structure was solved by direct methods (SHELXS-97) and refined against F^2 using SHELXL-97.^{27,28} Subsequent difference Fourier syntheses led to the location of all remaining nonhydrogen atoms. For the structure refinement, all data were used including negative intensities. All nonhydrogen atoms were refined anisotropically if not remarked upon otherwise below. Hydrogen atoms were idealized with the standard SHELX idealization methods. The program SADABS²⁹ was applied for the absorption correction. Complete crystallographic details, atomic coordinates, anisotropic thermal parameters, and fixed hydrogen atom coordinates are given in the Supporting Information; a brief summary of crystallographic details is given in Table 1.

[Fe(MbenTpivPP)(1-MeIm)₂]\cdot 1-MeIm. A translucent, red, plate crystal with the dimensions of $0.02 \times 0.02 \times 0.01 \text{ mm}^3$ was used for the structure determination. The asymmetric unit contains one bis-ligated [Fe(MbenTpivPP)(1-MeIm)₂] porphyrin complex and one 1-methylimidazole molecule. All the atoms are ordered including the *tert*-butyl “picket” atoms and the 1-MeIm solvent molecule. All nonhydrogen atoms were refined anisotropically.

Mössbauer spectra measurement.

Mössbauer measurements were performed on a constant acceleration spectrometer from 25 to 295 K with optional small field (Knox College). The 95% ⁵⁷Fe-enriched [⁵⁷Fe(MbenTpivPP)Cl] were prepared by a method similar to that of Landergrén.³⁰ Dark red powder of [⁵⁷Fe(MbenTpivPP)(1-MeIm)₂] was obtained by slow addition of hexanes to a reduced benzene solution of [⁵⁷Fe(MbenTpivPP)] and excess 1-MeIm as noted above. The product was dried in vacuum for 8 h and immobilized with a minimum of Apiezon M grease. The sample holder was sealed and used immediately for Mössbauer characterization. A sampling of spectra over the temperature range are given in the Supporting Information.

Results

The synthesis of a new modified “picket fence” porphyrin and its iron derivatives are reported. The six-coordinate final product [Fe(MbenTpivPP)(1-MeIm)₂] is characterized by UV-vis, single crystal X-ray and Mössbauer spectra. The ¹H, ¹³C-¹H NMR spectra and UV-vis spectra are given in Supporting Information. Two labeled Oak Ridge thermal ellipsoid plot (ORTEP) diagrams of [Fe(MbenTpivPP)(1-MeIm)₂] with views perpendicular or parallel to the porphyrin planes are given in Figures 1 and 2. Additional quantitative information is given in Figure 3. A brief summary of the crystallographic data is given in Table 1.

Solid-state Mössbauer spectra were measured for [⁵⁷Fe(MbenTpivPP)(1-MeIm)₂] and taken at several different temperatures from 25 to 295 K; they will be discussed subsequently.

Table 1. Complete Crystallographic Details for [Fe(MbenTpivPP)(1-MeIm)₂]\cdot 1-MeIm

	[Fe(MbenTpivPP)(1-MeIm) ₂]\cdot 1-MeIm
chemical formula	C ₇₈ H ₇₈ FeN ₁₄ O ₄
fw	1332.40
<i>a</i> , Å	22.6252(15)
<i>b</i> , Å	15.1697(9)
<i>c</i> , Å	20.6703(12)
α , deg	90
β , deg	101.996(2)
γ , deg	90
<i>V</i> , Å ³	6939.5(7)
space group	<i>P</i> 2 ₁ / <i>c</i>
<i>Z</i>	4
temp, K	150
<i>D</i> _{calcd} , g cm ⁻³	1.275
μ , mm ⁻¹	0.279
Final <i>R</i> indices	<i>R</i> ₁ = 0.0582
[<i>I</i> > 2 σ (<i>I</i>)]	<i>wR</i> ₂ = 0.1343
Final <i>R</i> indices	<i>R</i> ₁ = 0.0841
(all data)	<i>wR</i> ₂ = 0.1472

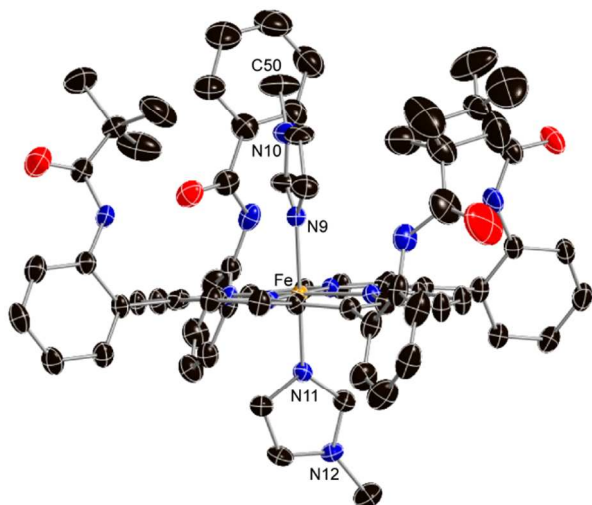


Figure 1. A edge-on ORETP diagram of $[\text{Fe}(\text{MbenTpivPP})(1\text{-Melm})_2]$ displaying the atom labeling scheme. Thermal ellipsoids of all atoms are contoured at the 40% probability level. Hydrogen atoms have been omitted for clarity. The porphyrin plane is perpendicular to the plane of the paper.

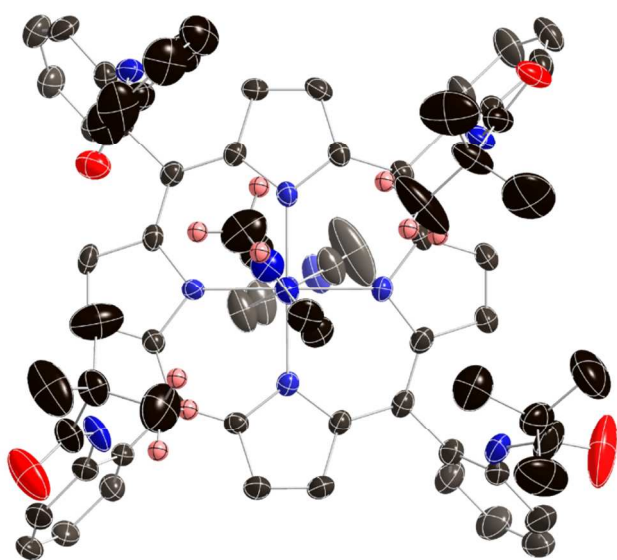


Figure 2. A top-down ORETP diagram of $[\text{Fe}(\text{MbenTpivPP})(1\text{-Melm})_2]$. Thermal ellipsoids of all atoms are contoured at the 40% probability level. The porphyrin plane is in the plane of the paper.

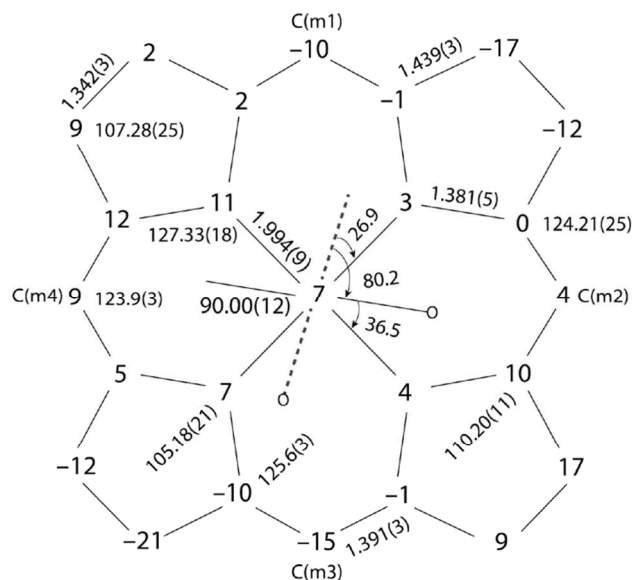


Figure 3. A Formal diagram of the porphyrinato core of $[\text{Fe}(\text{MbenTpivPP})(1\text{-Melm})_2]$. Averaged values of the chemically unique bond distances (in Å) and angles (in degree) are shown. The numbers in parentheses are the esd's calculated on the assumption that the averaged values were all drawn from the same population. The perpendicular displacements (in units of 0.01 Å) of the porphyrin core atoms from the 24-atom mean plane are also displayed. Positive values of the displacement are towards the hindered porphyrin side. The dashed line indicates the imidazole on the unhindered porphyrin side and the circle represents the position of the methyl group on axial ligand.

Discussion

Synthesis.

Since the report of “picket fence” porphyrin on “synthetic models of oxygen-binding hemoproteins,”³¹ many analogues have been brought forward including the “tailed picket fence”,²⁶ “pocket”,³² “picnic basket”,³³ porphyrins and others.³⁴ Several synthetic routes have been reported on the preparation of modified picket fence porphyrins, where one of the *t*-butyl pickets is substituted by a functional group to produce an asymmetric pocket environment. In the method reported by Reed and co-workers,³⁵ H_2TamPP is at first protected by one equivalent of triphenylmethyl group which will be removed after the addition of three pivaloyl groups. Finally the fourth picket is introduced to yield the product. This method has been applied in the synthesis of some models.^{32,36} In an alternative method, H_2TamPP was treated with the major (3 eqv.) and minor (1 eqv.) substituents sequentially in a one-pot reaction and the resulting mixture was separated by column chromatography.³⁷ In this work, we prepared $\text{H}_2\text{MbenTpivPP}$ porphyrin in two steps (Scheme 1). H_2TamPP was first reacted with three equivalents of pivaloyl chloride to yield the intermediate product of $\text{H}_2\text{MamTpivPP}$. In the second step, a phenyl group is introduced by the reaction of benzoyl chloride with $\text{H}_2\text{MamTpivPP}$.

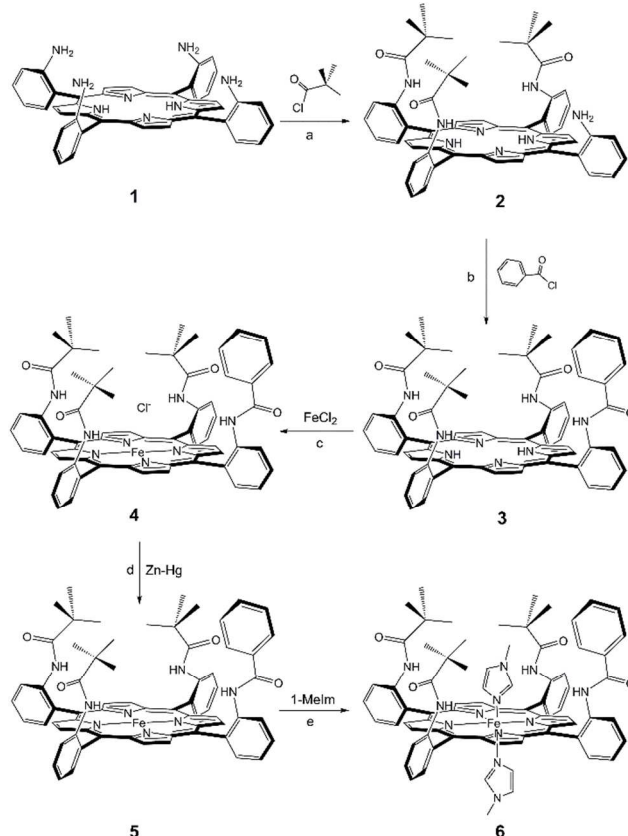
$[\text{Fe}(\text{MbenTpivPP})\text{Cl}]$ is yielded by the metalation of $\text{H}_2\text{MbenTpivPP}$ with FeCl_2 . Crystalline $[\text{Fe}(\text{MbenTpivPP})(1\text{-$

MeIm)₂] can be isolated by slow diffusion of hexanes to a benzene solution of [Fe(MbenTpivPP)] containing excess amount of 1-MeIm. As a modified “picket fence” porphyrin, the UV-vis spectra of [Fe(MbenTpivPP)Cl] (CHCl₃: 417, 506, 577, 645, 674 nm) and [Fe(MbenTpivPP)(1-MeIm)₂] (Benzene: 429, 536, 563 nm) are very similar to the corresponding picket fence analogues of [Fe(TpivPP)Cl] (CHCl₃: 418, 508, 578, 648, 675 nm) and [Fe(TpivPP)(1-MeIm)₂] (Benzene: 429, 535, 565 nm). In addition, the UV-vis spectra of [Fe(MbenTpivPP)(Py)₂] and the carbonyl product [Fe(MbenTpivPP)(CO)(1-MeIm)] are also similar to those of the traditional picket fence porphyrins.³¹ These will be found in the Supporting Information.

Structure.

We have characterized the single crystal X-ray structure of [Fe(MbenTpivPP)(1-MeIm)₂]. Two ORTEP diagrams have been presented. Figure 1 gives the view parallel to the porphyrin plane, whereas Figure 2 is the top-down view. It can be seen that the two imidazole ligands are perpendicular to the porphyrin plane, and the two imidazole planes have a relative perpendicular orientation. The 1-MeIm ligand plane on the hindered porphyrin side makes a dihedral angle of 36.5°; the imidazole on the other side making a 26.9° angle to the closest Fe—N_p vector. The dihedral angle between the two imidazole planes is 80.2°. The methyl group of the 1-MeIm on the hindered porphyrin side points to the benzene group on one of the four pickets, and the imidazole and benzene planes are near perpendicular to each other with the dihedral angle being 84.3°.

Scheme 1 The Synthesis of [Fe(MbenTpivPP)(1-MeIm)₂]^a



^a Conditions: (a) 2,6-lutidine, CH₂Cl₂, r.t., 8 h; (b) 2,6-lutidine, CH₂Cl₂, r.t., overnight; (c) 2,6-lutidine, chlorobenzene, 65 °C, 10 h; (d) benzene, r.t., overnight; (e) benzene, r.t., 1 h.

Additional quantitative information of the molecular structure is given in Figure 3, which displays the detailed displacements of the porphyrin core atom (in units of 0.01 Å) from the 24-atom mean plane. The orientations of the two 1-MeIm ligands including the values of the dihedral angles are also shown; the circle represents the position of the methyl group on the axial ligand. Figure 3 shows that the complex has a near planar porphyrin core conformation. The β carbon atoms have the largest displacements (0.21 and 0.17 Å). The iron center is slightly out of the mean plane (0.07 Å) towards the hindered porphyrin side. This is similar to the three “picket fence” analogues of [FeTpivPP(R-Im)₂] (R-Im = 1-MeIm, 1-EtIm and 1-VinylIm) where the iron atoms show out of plane distances ~ 0.05 Å towards the hindered porphyrin sides.¹⁹ The N_p—Fe—N_p angle is ideal at 90.00(12)°. The average Fe—N_p distance of 1.994(9) Å is a typical value for low-spin (porphinato)iron(II) derivatives.¹ Although most of these structural features are expected for low-spin [Fe(II)(Porph)(Im)₂] complexes with non-steric imidazole ligands, one feature was quite unexpected: the absolute and mutual orientations of the two imidazole rings. This distinctive feature makes [Fe(MbenTpivPP)(1-MeIm)₂] a new type among its analogues.

The key structural parameters of all structurally characterized [Fe(II)(Porph)(L)₂] (L: planar nitrogen donor ligands) complexes are given in Table 2. The crystallographically required symmetry at the iron atom and the absolute ligand orientation given by the dihedral angle between the axial ligand's mean plane and the closest N_{ax}—Fe—N_p plane (conventionally denoted by φ) is listed in Table 2. Also given is the relative ligand orientation given by the dihedral angle between the two axial ligand's mean planes (denoted by θ).

Table 2. Selected Structural Parameters for [Fe(II)(Porph)(L)₂]^a

complex	Fe S. S. ^b	(Fe—N _p) _{av} ^{c,d}	Fe—N _{ax} ^d	(Fe—N _{ax}) _{av} ^{c,d}	Core conf. ^{d,e}	$\varphi_{1,2}$ ^{f,g}	θ ^{f,h}	Ref.
[Fe(MbenTpivPP)(1-Melm) ₂]	C ₁	1.994(9)	1.991(3) 1.986(3)	1.989	near-Pla (C _β ,0.12)	36.5 26.9	80.2	tw
[Fe(TpivPP)(1-Melm) ₂]	C ₁	1.992(3)	1.9958(19) 1.9921(18)	1.9940	near-Pla (C _m ,0.12)	8.5 21.1	77.2	19
[Fe(TpivPP)(1-EtIm) ₂]	C ₁	1.993(6)	2.0244(18) 1.9940(19)	2.0092	near-Pla (C _β ,0.05)	6.6 20.7	62.4	19
[Fe(TpivPP)(1-VinylIm) ₂]	C ₁	1.988(5)	1.9979(19) 1.9866(18)	1.9923	near-Pla (C _β ,0.17)	11.2 24.5	78.5	19
[Fe(TPP)(1-VinylIm) ₂]	C _i	2.001(2)	2.004(2)	2.004	near-Pla	14	0 ⁱ	18
[Fe(TPP)(1-BzylIm) ₂]	C _i	1.993(9)	2.017(4)	2.017	near-Pla	26	0 ⁱ	18
[Fe(TPP)(1-MeIm) ₂]	C _i	1.997(6)	2.014(5)	2.014	near-Pla	15	0 ⁱ	38
[Fe(TPP)(4-MeHIm) ₂]	C _i	1.9952(8)	2.0154(8)	2.0154	near-Pla	0.7	0 ⁱ	39
[Fe(TMP)(4-CNPy) ₂]	C _i	1.993(2)	1.996(2)	1.996	near-Pla	40	0 ⁱ	16
[Fe(TMP)(3-CNPy) ₂]	C _i	1.996(2)	2.026(2)	2.026	near-Pla	42	0 ⁱ	16
[Fe(TMP)(4-MePy) ₂]	C _i	1.988(2)	2.010(2)	2.010	near-Pla	41	0 ⁱ	16
[Fe(TPP)(Py) ₂]Py	C _i	1.993(6)	2.039(1)	2.039	near-Pla	34.4	0 ⁱ	40
[Fe(TPP)(Py) ₂]	C _i	2.001(2)	2.037(1)	2.037	near-Pla	45	0 ⁱ	41
[Fe(OEPOH)(Py) ₂](mol 1)	C _i	1.995(3)	2.017(4)	2.017	near-Pla	40.4	0 ⁱ	42
[Fe(OEPOH)(Py) ₂](mol 2)	C _i	1.997(6)	2.004(4)	2.004	near-Pla	43.3	0 ⁱ	42
[Fe(F ₈ TPP)(DCIm) ₂]	C _i	1.9905(6)	2.002(3)	2.002	near-Pla	14.1	0 ⁱ	43
[Fe(TMP)(2-MeHIm) ₂] (mol 1)	C ₁	1.964(5)	2.030(3) 2.047(3)	2.039	Ruf(0.51)	41.1 41.4	82.4	17
[Fe(TMP)(2-MeHIm) ₂] (mol 2)	C ₁	1.961(7)	2.032(3) 2.028(3)	2.030	Ruf(0.50)	44.8 37.9	84.4	17
Fe((C ₃ F ₇) ₄ P)(Py) ₂	C ₁	1.958(4)	2.007(6) 1.996(6)	2.002	Ruf(0.62)	41.3 46.0	87.5	44
[Fe(TF ₃ PPBr ₈)(Py) ₂]	C ₁	1.963(4)	2.007(7) 2.016(7)	2.012	Sad(0.97)	1.5 22.2	68.3	45
[Fe(TF ₃ PPCl ₈)(1-Melm) ₂]	C ₁	1.981(5)	1.999(5) 1.997(5)	1.998	Sad(0.82)	20.9 14.8	80.7	46
[Fe(<i>m</i> -OEP)(1-Melm) ₂]	C ₁	1.982(2)	2.000(2) 2.007(2)	2.0035	Sad(0.89)	32.2 23.8	80.9	47
[Fe(<i>m</i> -OEP)(1-Melm) ₂]·THF	C ₁	1.985(3)	1.999(3) 2.002(3)	2.0005	Sad(0.83)	30.0 30.3	89.8	47
[Fe(<i>m</i> -OEP)(Py) ₂] (mol 1)	C ₁	1.961(3)	1.991(3) 2.014(3)	2.0025	Sad(0.64)	38.2 44.2	84.5	48

ARTICLE						Journal Name		
[Fe(<i>m</i> -OEP)(Py) ₂]	C ₁	1.961(3)	1.999(3)	2.0080	Sad(0.85)	35.1	87.9	48
(mol 2)			2.017(3)			36.6		
[Fe(<i>m</i> -OEP)(3-ClPy) ₂]	C ₁	1.962(2)	1.989(2)	1.9990	Sad(0.80)	47.2	85.5	48
			2.009(2)			42.4		
[Fe(<i>m</i> -OEP)(4-CNPy) ₂]	C ₁	1.986(2)	2.014(2)	2.0145	Sad(0.91)	42.2	84.3	48
			2.015(2)			36.2		
[Fe(TPPBr ₄)(Py) ₂]	C ₂	1.976(2)	2.000(3)	2.020	Sad(0.67)	36.8	19.2	49
			2.040(3)			33.7		
[Fe(TPP)(Pyz) ₂]	C ₁	1.987(8)	2.010(3)	1.990	Sad(0.14)	3.9	40.9	50
			1.970(3)			37.0		

^a Estimated standard deviations are given in parentheses. ^b Site symmetry of Fe. ^c Averaged value. ^d Value in Å. ^e Number in parenthesis is the average displacement of the methine carbons (C_m) or pyrrole β carbons (C_β) from the 24-atom mean plane for ruffling (Ruf) or saddling (Sad) deformation, respectively; near-Pla indicates an almost planar porphyrin plane in a centrosymmetric or (modified) picket fence structures. ^f Value in degrees. ^g Dihedral angle between the plane of the closest N_p-Fe-N_{ax} and the ligand plane. ^h Dihedral angle between two axial ligands. ⁱ Exact value required by symmetry.

Excluding the current structure, there are a total of 28 iron(II) porphyrin structures in Table 2. Among these 28 structures, 12 structures possess crystallographically required inversion symmetry at iron atom and thus having relative parallel axial ligand pairs. These are the *Type I* porphyrin system. These structures also have near planar porphyrin planes consonant with the inversion symmetry. The last 13 species of Table 2 are the *Type II* porphyrin system which have no symmetry at iron (twelve) or C₂ symmetry (one). Most of them have large dihedral angles between the two axial ligands and all have strongly ruffled or saddled porphyrin cores which preclude the possibility of an inversion center. A combination of porphyrin peripheral groups, porphyrin plane conformation, and/or axial ligand substitution in these 13 derivatives are the reasons for the absence of the inversion center. These derivatives will be considered in turn.

In the structure of [Fe(TMP)(2-MeHIm)₂], a near perpendicular ligand orientation results from coordination of two bulky 2-methylimidazole ligands.¹⁷ The 2-methyl groups induce a strongly ruffled porphyrin core in which the ligands must bind in mutually perpendicular binding pockets if the iron center is to become low spin. The steric 2-MeHIm leads to longer Fe—N_{Im} bond distances relative to the other imidazole derivatives, as seen in Table 2. Electronic reasons for ruffling are precluded because the low spin d⁶ electron configuration of iron minimizes possible porphyrin → Fe π donation. This is contrast to the case of Fe(III) where the ground state is (d_{xz}, d_{yz})⁴(d_{xy})¹ and the porphyrin a_{2u} (π) → Fe(III) π donation requires ruffling.^{16,51} The six Fe(*m*-OEP)(L)₂ structures all have severely saddled porphyrin cores, resulting from the four bulky nitro groups at the *meso* positions.^{47,48} Three additional examples have a near-perpendicular ligand orientation: Fe((C₃F₇)₄P)(Py)₂,⁴⁴ [Fe(TF₅PPBr₈)(Py)₂]⁴⁵ and [Fe(TF₅PPCl₈)(1-MeIm)₂].⁴⁶ These three complexes have extremely ruffled (Fe((C₃F₇)₄P)(Py)₂) or saddled ([Fe(TF₅PPBr₈)(Py)₂] and [Fe(TF₅PPCl₈)(1-MeIm)₂]) core conformations. These porphyrin core conformations are the result of the peripheral substituents. The

last two examples have smaller dihedral angles between the two axial ligands; but both show saddled porphyrin cores.

Type III porphyrin systems are the three picket fence derivatives of [Fe(TpivPP)(R-Im)₂] (R-Im = 1-MeIm, 1-EtIm and 1-VinylIm), which feature with relatively perpendicular orientations of the two axial ligands as well as near planar porphyrin planes. The steric demands on the picket side of the porphyrin require the imidazole plane align along the Fe—N_p bond. All three derivatives have the two axial ligand planes with a relative perpendicular orientation. The systematic orientational behavior suggested that a modest π-bonding between the imidazoles and iron is maximized only if the two axial ligands have a relative perpendicular orientation.¹⁹

The modified picket fence structure shares some common features with the three traditional picket fence structures. 1) The Fe—N_{ax} bonds in the porphyrin pockets are longer than the same bonds at the other sides. 2) All the structures have near planar porphyrin planes with the iron centers slightly displaced to the hindered porphyrin sides. 3) The imidazole ligands at the unhindered porphyrin sides tend to have small angles (20.7~26.9°) with the closest Fe—N_p axes. Previously we have noted that in the six-coordinate picket fence porphyrin derivatives [Fe^{II}(TpivPP)(L₁)(Im)] (L₁ denotes the neutral ligand on the hindered side of the porphyrin plane), the dihedral angle between the imidazole rings and the closest Fe—N_p axis (φ₂) are in a narrow range of 20~24.5°, irrespective of the ligands (L₁) on the opposite sides.¹⁹ Scheidt and Chipman had suggested the interaction of imidazole pπ — metal pπ which would favor eclipsed orientations for both five- and six-coordinate imidazole-ligated complexes.⁵²

We now consider the second imidazole on the hindered porphyrin side. [Fe(MbenTpivPP)(1-MeIm)₂] presents a large φ₁ angle of 36.5°, in contrast to the small angles ~10° in [Fe(TpivPP)(R-Im)₂] (R-Im = 1-MeIm, 1-EtIm and 1-VinylIm) derivatives. This distinctive feature, together with the near planar porphyrin core and relative perpendicular ligand orientation, excludes [Fe(MbenTpivPP)(1-MeIm)₂] from the three types of porphyrin systems (*Type I*, *II* and *III*) noted

above. Then what bonding features led to the large φ_1 angle in $[\text{Fe}(\text{MbenTpivPP})(1\text{-MeIm})_2]$? Figure 4 illustrates the spacing-filling diagram of $[\text{Fe}(\text{MbenTpivPP})(1\text{-MeIm})_2]$; the diagram of $[\text{Fe}(\text{TpivPP})(1\text{-MeIm})_2]$ is also given for comparison. Both figures show the pocket porphyrin sides. It is seen that both porphyrins have strong steric effects on the orientation of axial ligands. The crowding between the axial imidazole and the bulky pickets allows a limited rotational motion of the axial ligand around the $\text{Fe}-\text{N}_{\text{Im}}$ bond. The axial ligand is forced to align in specific orientations, preventing the ligand plane from freely rotating. In $[\text{Fe}(\text{TpivPP})(1\text{-MeIm})_2]$ (right panel of Figure 4), the 1-MeIm is limited to near the $\text{Fe}-\text{N}_{\text{p}}$ axis and the methyl group is towards to the opening of the “V-shape” cavity of the pocket. This ligand alignment avoids the steric crowding from the bulky pickets. The other two structures of $[\text{Fe}(\text{TpivPP})(\text{R-Im})_2]$ ($\text{R-Im} = 1\text{-EtIm}$ and 1-VinylIm) show similar ligand orientations and all three structures have small φ_1 angles: 8.5° (1-MeIm), 6.6° (1-EtIm), and 11.2° (1-VinylIm).¹⁹ Whereas, $[\text{Fe}(\text{MbenTpivPP})(1\text{-MeIm})_2]$ presents a different situation (left panel of Figure 4). As can be seen, the 1-MeIm approximately bisects the $\text{N}_{\text{p}}-\text{Fe}-\text{N}_{\text{p}}$ angle and gives a large φ_1 angle of 36.5° . Although the “V-shape” cavity of the pocket exists there, the methyl group of 1-MeIm unexpectedly directs to the phenyl group on the substituted picket, which seems an unfavorable orientation. The two rings are almost perpendicular to each other with the dihedral angle being 84.3° . Such unusual assembly leads us to inspect the intramolecular interactions between the two groups.

Figure S1 (Supporting Information) depicts the crystallographic distances between 1-MeIm and phenyl groups. The distances between the methyl carbon atom (C_{50}) of 1-MeIm and the phenyl π plan is 3.660 \AA , slightly shorter than the sum (3.7 \AA) of the van der Waals radii of the methyl group (2.0 \AA) and aromatic carbon (1.7 \AA).⁵³ In addition, the distance between C_{50} and the centroid of benzene group ($d_{\text{C-X}}$) is 3.744 \AA , corresponding to the effective range for $\text{C}-\text{H}\cdots\pi$ interactions ($3.74\sim 3.93 \text{ \AA}$).⁵⁴ Thus, both distances suggest the intramolecular interactions between the two groups, which induced the special ligand orientations inside the porphyrin pocket. The $\text{C}-\text{H}\cdots\pi$ interaction, while weaker than the classical H bonding, plays noteworthy structure-stabilizing and structure-determining roles.⁵⁵

The larger φ_1 angle in $[\text{Fe}(\text{MbenTpivPP})(1\text{-MeIm})_2]$ gives a more perpendicular mutual ligand orientation and larger θ angle ($\theta = 80.2^\circ$) than the traditional picket fence structures $[\text{Fe}(\text{TpivPP})(\text{R-Im})_2]$ ($\text{R-Im} = 1\text{-MeIm}$, 1-EtIm and 1-VinylIm). Figure 5 shows the correlation between the mutual ligand orientation θ angles and the averaged $\text{Fe}-\text{N}_{\text{Im}}$ bond distances ($(\text{Fe}-\text{N}_{\text{Im}})_{\text{av}}$) of the four picket fence porphyrinates. It is seen that the two parameters show a negative correlation that more perpendicular mutual ligand orientations correspond to shorter $(\text{Fe}-\text{N}_{\text{Im}})_{\text{av}}$ distances. $[\text{Fe}(\text{MbenTpivPP})(1\text{-MeIm})_2]$ shows the largest θ angle and the strongest $\text{Fe}-\text{N}_{\text{Im}}$ bond among the four complexes. Given the same filled $d\pi$ orbitals of the low-spin d^6 iron centers which would stabilize the axial

ligand bonds through iron $d\pi \rightarrow$ imidazole $p\pi$ back-bonding, Figure 5 demonstrates such a correlation that the π bonding interaction is enhanced with the increase of mutual ligand orientation.

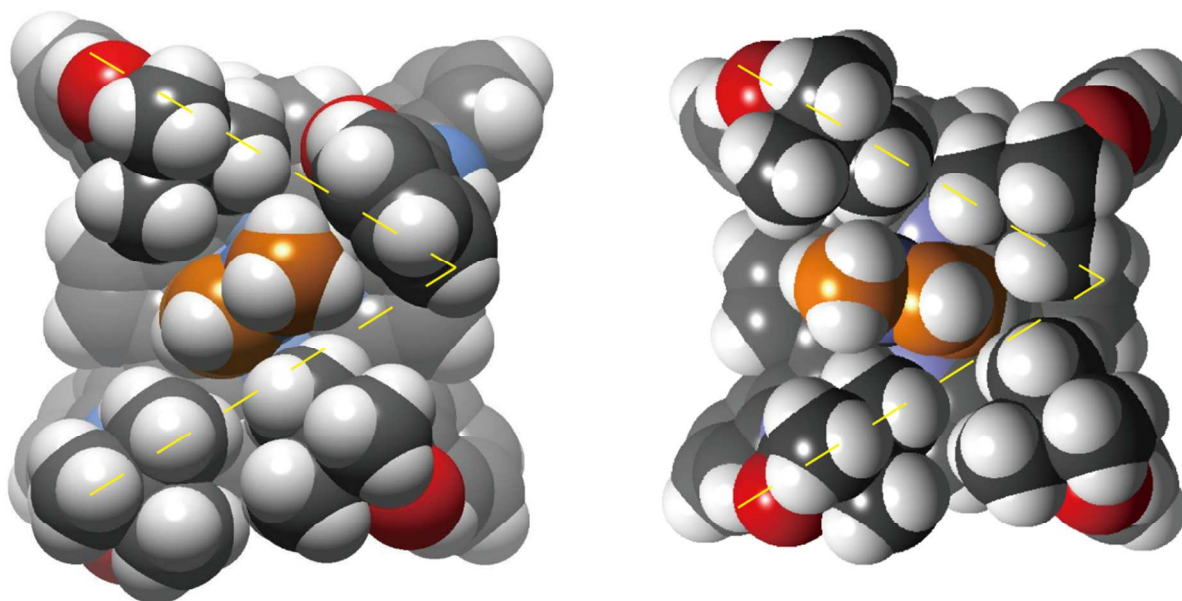


Figure 4. Spacing-filling diagrams (viewed perpendicular to the porphyrin plane) of [Fe(MbenTpivPP)(1-MeIm)₂] (left) and [Fe(TpivPP)(1-MeIm)₂] (right), showing the pocket porphyrin side (Carbon, dark grey; imidazole carbon, brown; Hydrogen, light grey; Nitrogen, blue; Oxygen, red; drawn with CrystalMaker).

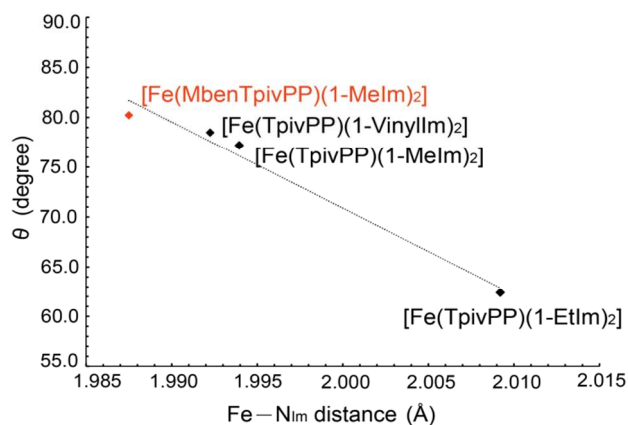


Figure 5. Correlation between mutual ligand orientation (θ angles) and the average Fe-N_{im} bond distances of [Fe(MbenTpivPP)(1-MeIm)₂] and [Fe(TpivPP)(R-Im)₂] (R-Im = 1-MeIm, 1-EtIm and 1-Vinylim) structures

It had been assumed that for the closed subshell configuration of low-spin d⁶ Fe(II) porphyrinates, planar axial ligands would prefer to align themselves in mutually perpendicular orientations to maximize the π -bonding interactions between the filled d_{z²} orbitals of Fe(II) and the π^* orbitals of the ligands. However this expected result was not forthcoming. In contrast, investigations showed low-spin Fe(II) porphyrinates preferred to have planar axial ligands oriented parallel to each other, and that π -bonding between Fe(II) and the axial ligands are minimal,¹⁶ as observed in the *Type I* porphyrin system that noted above. Recently in the study of picket fence [FeTpivPP(R-Im)] complexes, we were interested to see both

structural characteristics of near perpendicular ligand orientation and near planar porphyrin core which had been expected for the simple porphyrin models. The investigation suggested modest π -bonding between the imidazole and iron. In this work, the iron d π \rightarrow imidazole p π back-bonding is rationalized through a quantitative change of axial bond distances upon the mutual ligands orientations. The π -bonding is sensitive to the mutual ligand orientation, such that more perpendicular ligand orientations correspond to shorter axial ligand distances and stronger π -bonding interactions.

Mössbauer spectra.

Mössbauer spectra were measured for [Fe(MbenTpivPP)(1-MeIm)₂] in the solid state from room temperature to 25 K (Figure 6 and Figure S5, Supporting Information). The data were fit to four overlapped Lorentzian lines for each temperature. According to the 25 K spectrum (Figure 6), the major component is 91% occupied. The quadrupole splitting (ΔE_Q) decreases slightly with decreasing temperature with a maximum value of 1.05 mm/s at room temperature and a minimum of 0.98 mm/s at 25 K. The isomer shift increases slightly from 0.35 to 0.43 mm/s (Table 3). Both the quadrupole splitting and the isomer shift values are those expected for a low-spin iron(II) complex. The minor component is presumed to be a bis(imidazole) ligated, low spin ferric complex of [Fe(MbenTpivPP)(1-MeIm)₂]⁺, according to its isomer shift and quadrupole splitting values.^{2,56}

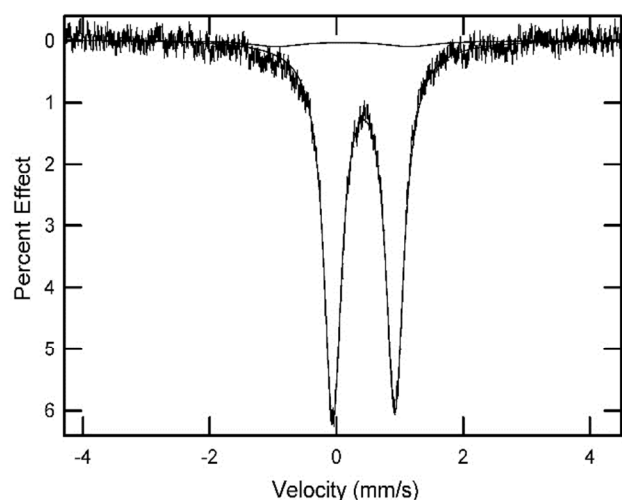


Figure 6. Mössbauer spectrum of $[\text{Fe}(\text{MbenTpivPP})(1\text{-MeIm})_2]$ at 25 K.

Table 3 gives the Mössbauer data of all known, six-coordinate low-spin species of $[\text{Fe}(\text{II})(\text{Porph})(\text{L})_2]$, also given are the relative ligand orientation and porphyrin core conformations. The upper entries shows the Mössbauer data observed for the current complex and the values observed for picket fence analogues of $[\text{Fe}(\text{TpivPP})(\text{R-Im})_2]$ ($\text{R-Im} = 1\text{-MeIm}, 1\text{-EtIm}$ and 1-VinylIm). It is seen that the ΔE_Q and δ parameters of these species are very consistent with each other; all complexes have quadrupole splitting values in the narrow range of 0.98~1.07 mm/s, and the isomer shift in 0.35~0.44 mm/s, which suggest the similarity between them. The 15 complexes of middle table entries are different from the traditional/modified picket fence complexes in the parallel ligand orientation. However the last four complexes with ΔE_Q larger than 1.5 mm/s all have ruffled porphyrin cores. Previously we have claimed that for low-spin $[\text{Fe}(\text{II})(\text{Porph})(\text{L})_2]$ derivatives the common geometric feature for a large quadrupole splitting ($\Delta E_Q \geq 1.5$ mm/s) is a ruffled core conformation and not the ligand orientation.¹⁹ The current study is certainly consistent with this conclusion.

Table 3. Selected Mössbauer Parameters for $[\text{Fe}(\text{II})(\text{Porph})(\text{L})_2]$ Derivatives

complex	ΔE_Q^a	δ_{Fe}^a	sample phase	T, K	θ^b	conf. ^c	ref.
$[\text{Fe}(\text{MbenTpivPP})(1\text{-MeIm})_2]$	0.98	0.43	cryst solid	25	80.2	near-Pla	tw
	0.99	0.42		100			
	1.01	0.40		200			
	1.05	0.35		295			
$[\text{Fe}(\text{TpivPP})(1\text{-MeIm})_2]$	0.99	0.44	cryst solid	20	77.2	near-Pla	19
	1.00	0.43		100			
	1.02	0.42		200			
	1.05	0.35		298			
$[\text{Fe}(\text{TpivPP})(1\text{-EtIm})_2]$	1.03	0.45	cryst solid	20	64.3	near-Pla	19
	1.04	0.44		100			
	1.05	0.42		200			
	1.07	0.37		298			
$[\text{Fe}(\text{TpivPP})(1\text{-VinylIm})_2]$	1.02	0.43	cryst solid	20	78.6	near-Pla	19
	1.02	0.42		100			
	1.03	0.41		200			
	1.07	0.35		298			
$[\text{Fe}(\text{TPP})(1\text{-MeIm})_2]$	1.07	0.47	cryst solid	77	0	near-Pla	18
$[\text{Fe}(\text{TPP})(1\text{-VinylIm})_2]$	1.02	0.45	cryst solid	77	0	near-Pla	18
$[\text{Fe}(\text{TPP})(1\text{-BzylIm})_2]$	1.02	0.45	cryst solid	77	0	near-Pla	18
$[\text{Fe}(\text{TPP})(1\text{-AcIm})_2]$	0.97	0.45	cryst solid	77	<i>d</i>	<i>d</i>	18
$[\text{Fe}(\text{TPP})(1\text{-SiMe}_3\text{Im})_2]$	1.04	0.46	cryst solid	77	<i>d</i>	<i>d</i>	18
$[\text{Fe}(\text{TPP})(\text{Py})_2]$	1.15	0.40	cryst solid	77	0	near-Pla	57
$[\text{Fe}(\text{TMP})(4\text{-CNPY})_2]$	1.13	0.41	cryst solid	120	0	near-Pla	16
$[\text{Fe}(\text{TMP})(3\text{-ClPY})_2]$	1.23	0.43	cryst solid	120	0	near-Pla	16
$[\text{Fe}(\text{TMP})(4\text{-MePY})_2]$	1.12	0.42	cryst solid	120	0	near-Pla	16

[Fe(TMP)(4-NMePy) ₂]	1.27	0.36	cryst solid	120	0	near-Pla	16
[Fe(TMP)(1-MeIm) ₂]	1.11	0.43	cryst solid	120	<i>d</i>	<i>d</i>	16
[Fe(OEP)(1-MeIm) ₂]	0.96	0.46	frozen soln	77	<i>d</i>	<i>d</i>	58
[Fe(OEP)(4-NMe ₂ Py) ₂]	1.02	0.45	frozen soln	77	<i>d</i>	<i>d</i>	58
[Fe(OEP)(4-CNPy) ₂]	1.10	0.32	frozen soln	77	<i>d</i>	<i>d</i>	58
[Fe(OEP)(Py) ₂]	1.13	0.46	cryst solid	4.2	<i>d</i>	<i>d</i>	59
[Fe(TMP)(2-MeHIm) ₂]	1.70	0.42	cryst solid	100	82.4/84.4	Ruf	17
[Fe(TMP)(2-MeHIm) ₂]	1.64	0.39	frozen soln	77	<i>e</i>	<i>e</i>	58
[Fe(OEP)(2-MeHIm) ₂]	1.67	0.34	frozen soln	77	<i>e</i>	<i>e</i>	58
[Fe(TMP)(1,2-Me ₂ Im) ₂]	1.73	0.39	frozen soln	77	<i>e</i>	<i>e</i>	58

^a mm/s. ^b Dihedral angle between two axial ligands, in degree. ^c Predominant core conformation contribution; Pla, planar; Ruf, ruffling. ^d Not determined, presumed parallel and planar. ^e Not determined, presumed perpendicular and ruffled.

Summary

A modified “picket fence” porphyrin and its iron complexes have been synthesized. The bis(imidazole)-ligated iron(II) porphyrin complex is studied by single-crystal X-ray, UV-vis and multi-temperature Mössbauer spectroscopy. The structure showed the largest relative ligand orientation among all the structurally characterized bis(imidazole)-ligated iron(II) porphyrinates with near planar porphyrin cores. The unusual ligand alignment inside the porphyrin pocket and the large dihedral angle to the nearest Fe—N_p vector is contributed to the combination of bulky pickets and the intramolecular C—H⋯π interactions. Investigations show the iron *d*π → imidazole *p*π back-bonding is sensitive to the mutual ligand orientation such that more perpendicular ligand orientations correspond to stronger π-bonding interactions (shorter axial ligand distances). Mössbauer spectra were obtained for the low spin title complex, which are consonant with the traditional picket fence analogues and confirmed our previous conclusion that the large quadrupole splitting values ($\Delta E_Q \geq 1.5$ mm/s) are associated with the porphyrin core conformation, rather than the relative axial ligand orientation.

Acknowledgements

We thank the CAS Hundred Talent Program and National Natural Science Foundation of China (Grant no. 21371167) to J.L.

Notes and references

^a College of Materials Science and Opto-electronic Technology, University of Chinese Academy of Sciences, YanQi Lake, HuaiRou District, Beijing, 101408, China

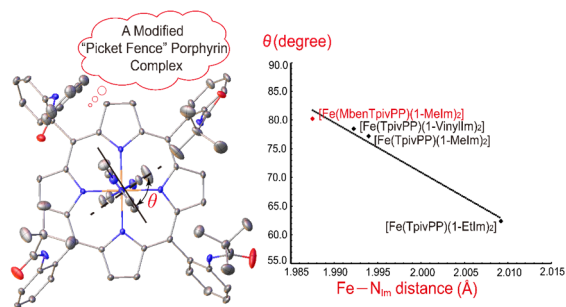
^b Department of Physics, Knox College, Galesburg, Illinois 61401, United States.

Electronic Supplementary Information (ESI) available: Crystallographic data in CIF format (CCDC 1051470); Figure S1 showing the crystallographic distances between 1-MeIm and phenyl groups of [Fe(MbenTpivPP)(1-MeIm)₂]. Figure showing UV-vis spectra (Fig. S2);

¹H NMR (Fig. S3) and ¹³C-¹H NMR spectra (Fig. S4) of H₂MbenTpivPP; multitemperature Mössbauer spectra (Fig. S5). See DOI: 10.1039/b000000x/

1. W. R. Scheidt and C. A. Reed, *Chem. Rev.*, 1981, **81**, 543.
2. F. A. Walker, *Chem. Rev.*, 2004, **104**, 589.
3. Abbreviations: Porph, a generalized porphyrin dianion; OEP, dianion of octaethylporphyrin; TTP, dianion of *meso*-tetratolylporphyrin; MbenTpivPP, dianion of *meso*-mono[*o*-o-(benzenecarboxamido)phenyl]tris(*o*,*o*,*o*-pivalamidophenyl)porphyrin; TpivPP, dianion of *o*,*o*,*o*,*o*-tetrakis(*o*-pivalamidophenyl)porphyrin; TPP, dianion of *meso*-tetraphenylporphyrin; TMP, dianion of *meso*-tetramesitylporphyrin; F₈TPP, dianion of *meso*-tetrakis(2,6-difluorophenyl)porphyrin; ((C₃F₇)₄)P, dianion of 5,10,15,20-tetrakis(heptafluoropropyl)porphyrin; TF₅PPBr₈, dianion of 2,3,7,8,12,13,17,18-octabromo-5,10,15,20-tetrakis(pentafluorophenyl)porphyrin; TPPBr₄, dianion of 2,3,12,13-tetrabromo-5,10,15,20-tetraphenylporphyrin; *m*-OEP, dianion of 2,3,7,8,12,13,17,18-octaethyl-5,10,15,20-tetranitroporphyrin; TF₅PPCl₈, dianion of 2,3,7,8,12,13,17,18-octachloro-5,10,15,20-tetrakis(pentafluorophenyl)porphyrin; OEPOH, dianion of octaethyl-*meso*-hydroxyporphyrin. Axial ligand: HIm, imidazole; 1-MeIm, 1-methylimidazole; 2-MeHIm, 2-methylimidazole; 4-MeHIm, 4-methylimidazole; 1,2-Me₂Im, 1,2-dimethylimidazole; 1-AcIm, 1-acetylimidazole; 1-SiMe₃Im, 1-(trimethylsilyl)imidazole; 1-VinylIm, 1-vinylimidazole; 1-BzylIm, 1-benzylimidazole; DCIm, 1,5-dicyclohexyl; Im, generalized imidazole; Py, pyridine; 3-ClPy, 3-chloropyridine; 4-CNPy, 4-cyanopyridine; 3-CNPy, 3-cyanopyridine; 4-MePy, 4-methylpyridine; 4-NMe₂Py, 4-(dimethylamino)pyridine; Pyz, pyrazine. Other: THF, tetrahydrofuran; N_p, porphyrinato nitrogen; N_{ax}, nitrogen of axial ligands; EPR, electron paramagnetic resonance; NMR, nuclear magnetic resonance; UV-vis, Ultraviolet-visible.
4. W. R. Scheidt and D. K. Geiger, *J. Chem. Soc., Chem. Commun.*, 1979, 1154.
5. W. R. Scheidt, D. K. Geiger and K. J. Haller, *J. Am. Chem. Soc.*, 1982, **104**, 495.
6. W. R. Scheidt, D. K. Geiger, R. G. Hayes and G. Lang, *J. Am. Chem. Soc.*, 1983, **105**, 2625.
7. F. A. Walker, *Coord. Chem. Rev.*, 1999, 471.
8. O. Q. Munro, H. M. Marques, P. G. Debrunner, K. Mohanrao and W. R. Scheidt, *J. Am. Chem. Soc.*, 1995, **117**, 935.

9. M. K. Safo, G. P. Gupta, F. A. Walker and W. R. Scheidt, *J. Am. Chem. Soc.*, 1991, **113**, 5497.
10. M. K. Safo, G. P. Gupta, C. T. Watson, U. Simonis, F. A. Walker and W. R. Scheidt, *J. Am. Chem. Soc.*, 1992, **114**, 7066.
11. F. A. Walker, D. Reis and V. L. Balke, *J. Am. Chem. Soc.*, 1984, **106**, 6888.
12. C. T. Migita and M. Iwaizumi, *J. Am. Chem. Soc.*, 1981, **103**, 4378.
13. (a) W. R. Scheidt, J. F. Kirner, J. L. Hoard and C. A. Reed, *J. Am. Chem. Soc.*, 1987, **109**, 1963; (b) F. A. Walker, B. H. Huynh, W. R. Scheidt and S. R. Osvath, *J. Am. Chem. Soc.*, 1986, **108**, 5288.
14. W. R. Scheidt, S. R. Osvath and Y. J. Lee, *J. Am. Chem. Soc.*, 1987, **109**, 1958.
15. (a) O. Q. Munro, J. A. Serth-Guzzo, I. Turowska-Tyrk, K. Mohanrao, T. K. Shokhireva, F. A. Walker, P. G. Debrunner and W. R. Scheidt, *J. Am. Chem. Soc.*, 1999, **121**, 11144; (b) R. Quinn, J. S. Valentine, M. P. Byrn and C. E. Strouse, *J. Am. Chem. Soc.*, 1987, **109**, 3301.
16. M. K. Safo, M. J. M. Nettet, F. A. Walker, P. G. Debrunner and W. R. Scheidt, *J. Am. Chem. Soc.*, 1997, **119**, 9438.
17. C. Hu, B. C. Noll, C. E. Schulz and W. R. Scheidt, *Inorg. Chem.*, 2005, **44**, 4346.
18. M. K. Safo, W. R. Scheidt and G. P. Gupta, *Inorg. Chem.*, 1990, **29**, 626.
19. J. Li, S. M. Nair, B. C. Noll, C. E. Schulz and W. R. Scheidt, *Inorg. Chem.*, 2008, **47**, 3841.
20. (a) J. P. Collman, R. R. Gagne, C. A. Reed, W. T. Robinson and G. A. Rodley, *Proc. Natl. Acad. Sci. U.S.A.*, 1974, **71**, 1326; (b) J. P. Collman, J. I. Brauman, E. Rose and K. S. Suslick, *Proc. Natl. Acad. Sci. U.S.A.*, 1978, **75**, 1052.
21. (a) H. Imai, S. Sekizawa and E. Kyuno, *Inorg. Chim. Acta*, 1986, **125**, 151; (b) H. Imai, S. Nakagawa and E. Kyuno, *Inorg. Chim. Acta*, 1992, **193**, 105.
22. G. E. Wuenschell, C. Tetreau, D. Lavalette and C. A. Reed, *J. Am. Chem. Soc.*, 1992, **114**, 3346.
23. J. Li, Q. Peng, A. Barabanschikov, J. W. Pavlik, E. E. Alp, W. Sturhahn, J. Zhao, C. E. Schulz, J. T. Sage and W. R. Scheidt, *Chem.—Eur. J.*, 2011, **17**, 11178.
24. J. Li, B. C. Noll, A. G. Oliver, C. E. Schulz and W. R. Scheidt, *J. Am. Chem. Soc.*, 2013, **135**, 15627.
25. J. Lindsey, *J. Org. Chem.*, 1980, **45**, 5215.
26. J. P. Collman, J. I. Brauman, K. M. Doxsee, T. R. Halbert, E. Bunnenberg, R. E. Linder, G. N. LaMar, J. Del Gaudio, G. Lang and K. Spartalian, *J. Am. Chem. Soc.*, 1980, **102**, 4182.
27. G. M. Sheldrick, *Acta Crystallogr., Sect. A*, 2008, **64**, 112.
28. $R_1 = \sum ||F_o| - |F_c|| / \sum |F_o|$ and $wR_2 = \{ \sum [w(F_o^2 - F_c^2)^2] / \sum [wF_o^4] \}^{1/2}$. The conventional R -factors R_1 are based on F , with F set to zero for negative F^2 . The criterion of $F^2 > 2 \sigma(F^2)$ was used only for calculating R_1 . R -factors based on F^2 (wR_2) are statistically about twice as large as those based on F , and R -factors based on all data will be even larger.
29. G. M. Sheldrick, *Program for Empirical Absorption Correction of Area Detector Data*, Universität Göttingen, Germany, 1996.
30. M. Landergrén and L. Baltzer, *Inorg. Chem.*, 1990, **29**, 556.
31. J. P. Collman, R. R. Gagne, C. A. Reed, T. R. Halbert, G. Lang and W. T. Robinson, *J. Am. Chem. Soc.*, 1975, **97**, 1427.
32. J. P. Collman, J. I. Brauman, T. J. Collins, B. L. Iverson, G. Lang, R. B. Pettman, J. L. Sessler and M. A. Walters, *J. Am. Chem. Soc.*, 1983, **105**, 3038.
33. J. P. Collman, X. Zhang, K. Wong and J. I. Brauman, *J. Am. Chem. Soc.*, 1994, **116**, 6245.
34. J. P. Collman, R. Boulatov, C. J. Sunderland and L. Fu, *Chem. Rev.*, 2004, **104**, 561.
35. G. E. Wuenschell, C. Tetreau, D. Lavalette and C. A. Reed, *J. Am. Chem. Soc.*, 1992, **114**, 3346.
36. (a) J. P. Collman, Y. L. Yan, J. P. Lei and P. H. Dinolfo, *Org. Lett.*, 2006, **8**, 923; (b) A. Nakagawa, T. Komatsu, M. Iizuka and E. Tsuchida, *Bioconjugate Chem.*, 2006, **17**, 146.
37. (a) H. Imai, A. Nakatsubo, S. Nakagawa, Y. Uemori and E. Kyuno, *Syn. React. Inorg. Met.*, 1985, **15**, 265; (b) K. Shigehara, K. Shinohara, Y. Sato and E. Tsuchida, *Macromolecules*, 1981, **14**, 1153.
38. W. L. Steffen, H. K. Chun, J. L. Hoard and C. A. Reed, *Abstr. Pap. Am. Chem. Soc.*, 1978, **175**, 15.
39. N. J. Silvernail, B. C. Noll and W. R. Scheidt, *Acta Crystallogr., Sect. E*, 2005, **61**, m1201.
40. N. Y. Li, V. Petricek and P. Coppens, *Acta Crystallogr. Sect. C—Cryst. Struct. Commun.*, 1985, **41**, 902.
41. N. Li, P. Coppens and J. Landrum, *Inorg. Chem.*, 1988, **27**, 482.
42. S. P. Rath, M. M. Olmstead and A. L. Balch, *Inorg. Chem.*, 2004, **43**, 6357.
43. H. R. Lucas, G. J. Meyer and K. D. Karlin, *J. Am. Chem. Soc.*, 2009, **131**, 13924.
44. K. T. Moore, J. T. Fletcher and M. J. Therien, *J. Am. Chem. Soc.*, 1999, **121**, 5196.
45. M. W. Grinstaff, M. G. Hill, E. R. Birnbaum, W. P. Schaefer, J. A. Labinger and H. B. Gray, *Inorg. Chem.*, 1995, **34**, 4896.
46. R. Patra, D. Sahoo, S. Dey, D. Sil and S. P. Rath, *Inorg. Chem.*, 2012, **51**, 11294.
47. R. Patra, A. Chaudhary, S. K. Ghosh and S. P. Rath, *Inorg. Chem.*, 2010, **49**, 2057.
48. R. Patra, S. Bhowmik, S. K. Ghosh and S. P. Rath, *Dalton Trans.*, 2010, **39**, 5795.
49. W. R. Scheidt and B. C. Noll, *Acta Crystallogr., Sect. E*, 2006, **62**, m1892.
50. W. Hiller, M. Hanack and M. G. Mezger, *Acta Crystallogr., Sect. C*, 1987, **C43**, 1264.
51. (a) M. K. Safo, F. A. Walker, A. M. Raitsimring, W. P. Walters, D. P. Dolata, P. G. Debrunner and W. R. Scheidt, *J. Am. Chem. Soc.*, 1994, **116**, 7760; (b) F. A. Walker, H. Nasri, I. Turowska-Tyrk, K. Mohanrao, C. T. Watson, N. V. Shokhirev, P. G. Debrunner and W. R. Scheidt, *J. Am. Chem. Soc.*, 1996, **118**, 12109.
52. W. R. Scheidt and D. M. Chipman, *J. Am. Chem. Soc.*, 1986, **108**, 1163.
53. (a) L. Pauling, *The Nature of the Chemical Bond*, Cornell University Press, Ithaca, N.Y., 1960; (b) A. Bondi, *J. Phys. Chem.*, 1964, **68**, 441; (c) K. Jitsukawa, K. Iwai, H. Masuda, H. Ogoshi and H. Einaga, *J. Chem. Soc., Dalton Trans.*, 1997, **20**, 3691.
54. (a) H. Kooijman, A. L. Spek, H. Kleijn, H. L. v. Maanen, J. T. B. H. Jastrzebski and G. v. Koten, *Acta Crystallogr., Sect. C*, 2000, **56**, 481; (b) M. Brandl, M. S. Weiss, A. Jabs, J. Sühnel and R. Hilgenfeld, *J. Mol. Biol.*, 2001, **307**, 357.
55. (a) M. Nishio, M. Hirota and Y. Umezawa, *The CH/ π Interaction: Evidence, Nature, and Consequences*, Wiley, 1998; (b) E. A. Meyer, R. K. Castellano and F. Diederich, *Angew. Chem., Int. Ed.*, 2003, **42**, 1210.
56. C. Hu, B. C. Noll, C. E. Schulz and W. R. Scheidt, *Inorg. Chem.*, 2006, **45**, 9721.
57. H. Kobayashi, Y. Maeda and Y. Yanagawa, *Bull. Chem. Soc. Jpn.*, 1970, **43**, 2342.
58. J. R. Polam, J. L. Wright, K. A. Christensen, F. A. Walker, H. Flint, H. Winkler, M. Grodzicki and A. X. Trautwein, *J. Am. Chem. Soc.*, 1996, **118**, 5272.
59. D. Dolphin, J. R. Sams, T. B. Tsin and K. L. Wong, *J. Am. Chem. Soc.*, 1976, **98**, 6970.



The synthesis and characterization of [Fe(MbenTpivPP)(1-MeIm)₂], a new species among bis(imidazole) iron(II) porphyrinates, is reported. Investigations suggest the strong correlation between mutual ligand orientations (θ) and axial Fe—N_{Im} bond distances.